LA-UR-21-29753

Approved for public release; distribution is unlimited.

Title:	Calibration of the diffusivity predictions of Centipede using approximate Bayesian computation and applications in Nyx (engineering scale) and Xolotl-MARMOT (meso-scale) simulations
Author(s):	Pieterjan, Robbe; Casey, Tiernan; Matthews, Christopher; Cooper, Michael William Donald; Blondel, Sophie; Kim, Dong-Uk; Muntaha, Md Ali; Tonks, Michael; Wirth, Brian; Andersson, Anders David Ragnar; Najm, Habib; Pastore, Giovanni
Intended for:	Report
Issued:	2022-02-10 (rev.1)

Los Alamos
NATIONAL LABORATORY

Calibration of the diffusivity predictions of `Centipede` using approximate Bayesian computation and applications in `Nyx` (engineering scale) and `Xolotl`-`MARMOT` (meso-scale) simulations

Pieterjan Robbe[a], Tiernan Casey[a], Christopher Matthews[b], Michael Cooper[b], Sophie Blondel[c], Giovanni Pastore[c], Dong-Uk Kim[d], Md Ali Muntaha[d], Micheal Tonks[d], Brian Wirth[c], David Andersson[b], and Habib Najm[a]

[a]Sandia National Laboratories, Livermore, CA
[b]Los Alamos National Laboratory, Los Alamos, NM
[c]University of Tennessee, Knoxville, TN
[d]University of Florida, Gainesville, FL

September 2021

Abstract

Fission gas evolution and release in UO_2 nuclear fuel are important fuel performance metrics and occur in several distinct stages: 1) nucleation, growth and resolution of intra-granular bubbles, 2) diffusion to grain boundaries and 3) nucleation and growth of bubbles at grain boundaries, which eventually form a connected network (percolation) enabling release of gas from grain boundaries through connections to triple junctions, grain edges or free surfaces. The NE-SciDAC project is developing several computational tools to model this problem, which are connected in a hierarchical multi-scale framework. The information transfer in the multi-scale framework is a critical step that, in addition to best-estimates, should include uncertainty quantification. Despite taking a first-principles multi-scale approach, there is a need to perform parameter calibration to ensure consistency with available experimental data. In the present study, uncertainty quantification (UQ) and parameter calibration is demonstrated for one of the lower length scale codes in the multi-scale framework (`Centipede`) and then the results, including instances of the propagated uncertainties, are used in other codes within the framework, specifically `Nyx` and `Xolotl`-`MARMOT`.

We calibrated the model parameters in `Centipede`, a computer code used to predict diffusivities of uranium (U) and xenon (Xe) in the context of the simulation of fission gas in uranium oxide (UO_2) nuclear fuel. The `Centipede` code depends on 183 parameters, all of which are subject to uncertainty. The three data sets used in our calibration effort are taken from the literature, in particular references [1, 2, 3, 4]. This data is available

as a set of measurements, including measurement errors. Our goal is to calibrate a statistical model that predicts both the value of the measurement and the uncertainty associated with the measurement. We perform a Bayesian calibration of the model parameters using a dedicated *approximate Bayesian computation* (ABC) likelihood function. To avoid excessive computational costs, we replace the expensive `Centipede` simulation code by a higher-order surrogate model, constructed using only the 9 most important parameters. These important parameters are identified by a preliminary *global sensitivity analysis* (GSA) study. Among the important parameters are `T0` (the temperature at which UO_2 is perfectly stoichiometric) and `Hf_pO2` (the temperature dependence of the oxygen (O) partial pressure) that should be considered as operating conditions to be estimated along with the other parameters. We consider two different cases: one where we define one set of these operating conditions for all data sets, and one where we define distinct operating condition parameters for each data set. The Xe diffusivities predicted by the latter case show distinct features that could not be observed in the former.

Next, we use the diffusivity predictions by `Centipede` as input to `Nyx`, a reduced-order fuel performance code focused on gas behavior alone, in order to estimate quantities associated with inter-granular bubble formation at conditions specified by the experiments of [5]. Finally, the diffusivities obtained from the calibrated `Centipede` runs were used in coupled `Xolotl-MARMOT` simulations of intra- and inter-granular gas evolution. The results are compared to simulations using the baseline diffusivities from Turnbull et al. from [3].

Contents

1 Introduction, background and objectives

Fission gas evolution in UO_2 nuclear fuel progresses in several stages, as described in the literature based on experimental knowledge accumulated over several decades [6, 7, 8, 9, 10, 11, 12, 13]. Below, these stages are briefly summarized. Work performed under the current NE-SciDAC project to improve our understanding of the staged evolution of fission gas and to develop new capabilities to simulate the behavior is highlighted, with emphasis on providing background for uncertainty quantification (UQ), parameter calibration and a proof-of-principle uncertainty propagation exercise in the hierarchical multi-scale modeling and simulation framework used to describe fission gas evolution and release.

1.1 Fission gas evolution and release in UO_2

Xenon (Xe) atoms, which constitute the highest concentration among fission gases and are used as a representative case, are formed in fission events and initially come to rest in trap sites in the UO_2 lattice, of which the most stable is a cluster of uranium (U) and oxygen (O) vacancies [14, 15, 16, 17]. Due to their low solubility in the UO_2 lattice, there is a significant driving force for Xe atoms to escape by either nucleating and growing bubbles inside grains (intra-granular bubbles), on grain boundaries (inter-granular bubbles) or by escaping the fuel pellet entirely through release to the plenum. Nucleation and growth of intra-granular bubbles represent the first step in fission gas evolution and release. It is controlled by diffusion of individual gas atoms through the lattice, as described by the Xe diffusion coefficient. This diffusion coefficient is labeled the unperturbed Xe diffusivity as it excludes interactions with bubbles and other Xe sinks. However, the unperturbed diffusivity is influenced by interactions with point defects and, by extension, how the concentration of points defects is perturbed by irradiation. The diffusivity may also be impacted by impurities or other fission products, but accounting for those is considered future work. The preferred Xe trap site and active diffusion mechanism under thermal equilibrium and irradiation conditions were studied during the first few years of the NE-SciDAC project based on atomic scale simulations [14] and cluster dynamics simulations using the `Centipede` code [18, 15]. The resulting diffusion rates or diffusivities depend on complex interactions between point defects and Xe atoms, which result in a mechanistic diffusion model with many input parameters (183) that, in many cases, have substantial uncertainty. The present study will analyze those uncertainties and demonstrate how limited experimental data points on U and Xe diffusion may be used to refine mechanistic diffusion model parameters and improve the accuracy of model predictions.

The growth of intra-granular fission gas bubbles due to diffusion is counteracted by bubbles shrinking or being destroyed by fission fragments traveling through the lattice. In UO_2, most of the fission energy is dissipated by electronic stopping, which leads to a thermal spike in a localized region surrounding the fission fragment [19]. If a bubble is located in the sphere of influence of a thermal spike, it is either completely destroyed or a certain

fraction of gas atoms is knocked out of the fission gas bubble. Ballistic interaction between the fission gas fragment and the bubble has a similar effect, but is less prevalent than thermal spikes in UO_2. Based on large-scale molecular dynamics simulations, Ref. [19], which was generated under the NE-SciDAC pilot project, discusses the resolution processes in detail and develops a model of the resolution rate that is suitable for application in rate-theory models of gas evolution, such as those used in fuel performance codes and the `Xolotl` cluster dynamics code [20, 21, 22, 23, 24].

The balance between growth of bubbles due to diffusion and shrinkage or destruction due to fission fragments prevents the intra-granular bubbles from growing beyond a certain size and results in a steady-state distribution of nano-scale intra-granular bubbles. At high burnups, a bimodal distribution of intra-granular gas bubbles may still evolve, which is believed to be a consequence of more complex mechanisms than those described above, possibly related to pipe-diffusion along dislocations or sized-dependent growth/resolution rates [25]. The formation of a bimodal bubble distribution is researched separately under the NE-SciDAC project using both meso-scale `Xolotl` cluster dynamics simulations and engineering scale analysis [26].

Gas atoms may also diffuse through the lattice to grain boundaries, where fission gas bubbles grow much larger than within the grains due to more efficient capture mechanisms following interaction with fission fragments, which effectively turns off bubble resolution at grain boundaries. The rate at which gas atoms arrive at grain boundaries is controlled by the diffusion of Xe atoms through the lattice as well as the capture and resolution rate of Xe atoms by intra-granular bubbles. The net rate of arrival at grain boundaries is determined by an effective Xe diffusion coefficient, which is formulated in terms of the unperturbed bulk Xe diffusivity, the capture rate, which depends on the bulk diffusivity, and the bubble resolution rate. This is a simplified model suitable for engineering scale simulations of certain fuel conditions. However, it may not be valid for all conditions, in particular not for fuel exposed to high burnups or transients. In the NE-SciDAC project, these conditions are explored using spatially-resolved cluster dynamics simulations performed with the `Xolotl` code [20, 21, 22, 23, 24]. Segregation of gas to grain boundaries is considered the second step in the gas evolution and release process. Because grain boundary bubbles are not resolved by fission fragments, they will continue to grow as more gas arrive.

The third step in the gas evolution process is growth and interconnection of gas bubbles at grain boundaries. The bubbles eventually reach a percolation threshold that allows all gas at a boundary to connect with triple junctions, grain edges or free surfaces. The grain edges are typically assumed to be covered by gas bubbles earlier than grain face percolation occurs and to be connected with a free pellet surface, which allows the gas to be released to the plenum. Before reaching the percolation threshold at grain boundary faces and edges, these large bubbles contribute to gaseous swelling. In the NE-SciDAC project the evolution of gas bubbles on grain boundaries and grain edges is simulated with the `MARMOT` phase-field

5

code [27]. A key goal of the NE-SciDAC project is to couple the `Xolotl` and `MARMOT` codes, thus enabling representation of both intra- and inter-granular bubble evolution as well as diffusion and release of gas to the plenum.

1.2 Report objectives and structure

As described above, the NE-SciDAC project targets simulations of all steps in the fission gas evolution and release process. The ultimate objective is to develop an engineering scale model that accurately captures fission gas evolution and release at the pin scale for a range of operating conditions, which can only be accomplished by relying on mechanistic models at each length and time scale. At the outset of the NE-SciDAC project the necessary parts of such a methodology were identified, see Fig. 1 and discussion above. Uncertainty quantification has a critical role to play in connecting the scales through propagation of uncertainties and investigation of parameter sensitivities. Another important component of uncertainty quantification is the ability to calibrate parameters in the mechanistic models of gas evolution based on experimental data available on macro-scale properties, such as diffusion coefficients and thermodynamic equilibrium data. These allow incorporation of knowledge acquired in historical gas release and thermodynamic experiments into advanced models, while still maintaining the benefits of mechanistic models derived from more recent atomic and meso-scale scale simulations. The purpose of the present report is to provide a first demonstration of applying systematic uncertainty quantification to analyze mechanistic models relying on atomic scale data, refine or calibrate such models based on experimental data and propagate uncertainties in the hierarchical multi-scale framework set up to model fission gas evolution and release in the NE-SciDAC project.

The report is structured as follows. First, the atomic scale simulations performed to elucidate Xe diffusion mechanisms in irradiated UO_2 will be briefly summarized, which is followed by a summary of how this information is incorporated into the `Centipede` cluster dynamics code to calculate the irradiation response of point defects in UO_2 and how those determine the unperturbed Xe diffusivity in UO_2 nuclear fuel. Instead of applying the `Centipede` results in a full-fledged fuel performance code such as Bison, in the present study this step of the analysis will be performed based on a stand-alone code called `Nyx`. A brief summary of the `Nyx` code is also provided. The simulations performed in `Nyx` may easily be transferred to Bison once the development phase is complete. The calculated Xe diffusivity may also be used in the `Xolotl` and `MARMOT` codes as well as in coupled `Xolotl`-`MARMOT` simulations. The relevant methodology is highlighted. Following the review of the multi-scale methods to model gas evolution, the methodology and results from uncertainty quantification of the atomic scale parameters used by the `Centipede` code to calculate the unperturbed Xe diffusivity are summarized. In the next step, the atomic scale parameters used by `Centipede` are calibrated based on experimental measurements of U and Xe diffusivities available in the literature. The calibrated unperturbed Xe diffusivity is then used in the `Nyx` code to predict gas evolution at the fuel pin scale. These simulations also
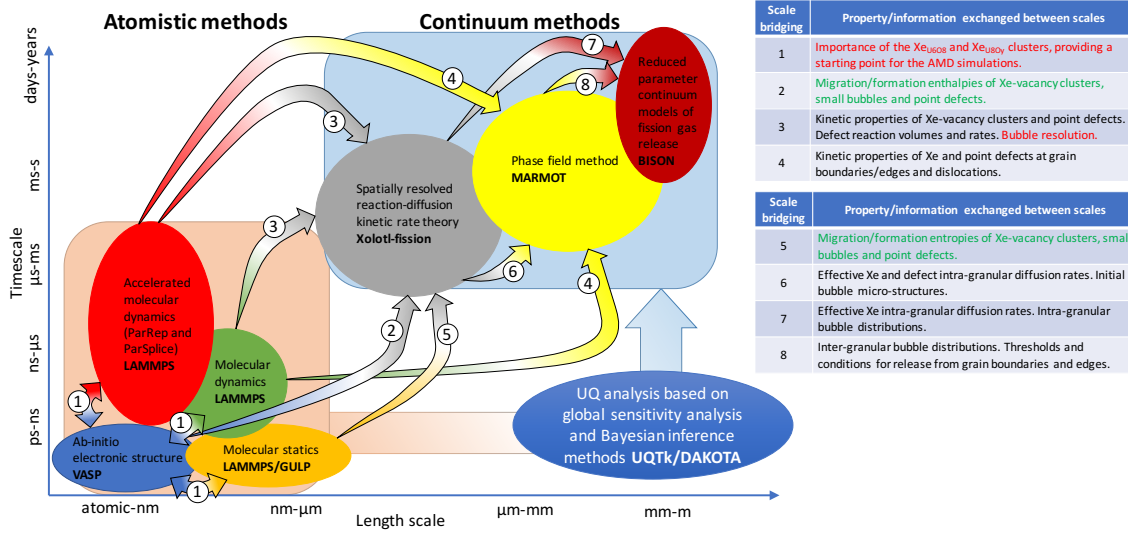
Figure 1: Multiscale framework used in the NE-SciDAC project to simulate fission gas evolution and release in UO_2. Uncertainty quantification has an important role in connecting atomic scale data with meso- and engineering scale simulation methods.

use the uncertainties propagated from the calibrated `Centipede` simulations. In addition, the unperturbed Xe diffusivities predicted by `Centipede` using the calibrated parameter set are used in `Xolotl-MARMOT` simulations to demonstrate the impact on fission gas evolution at the grain scale. The combined `Centipede`, `Nyx` and `Xolotl-MARMOT` exercises serve as a demonstration of incorporating uncertainties, performing calibration and validation against available experimental data in the hierarchical multi-scale simulation approach used in the NE-SciDAC project. Finally, our conclusions are presented.

2 Simulation methods for fission gas diffusion, evolution and release in UO_2

2.1 Diffusivities under thermal equilibrium conditions: Analytical models based on density functional theory and empirical potentials calculations

The first step in developing a mechanistic fission gas evolution and release model is to identify the active Xe diffusion mechanism under both thermal equilibrium and irradiation conditions. Ref. [14] calculated the thermodynamic (defect formation energies/entropies, binding energies/entropies) and kinetic properties (migration barriers, attempt frequencies) of Xe defect clusters involving up to ten U vacancies and sixteen O vacancies as well as for

interstitial defects that may contribute to diffusion. The calculations were performed based on density functional theory (DFT) for energies and semi-empirical potentials for entropies. In thermal equilibrium, the resulting Xe diffusivity may be calculated by weighting the diffusivity of each cluster by its relative concentration, as determined from an analytical point defect model. Ref. [14] shows that the resulting diffusivity agrees reasonably well with the experimental data due to Davies and Long [2], which is considered to be the most accurate data for application in fuel performance codes at high temperature, where irradiation effects are assumed to be negligible. The active diffusion mechanism refers to a Xe atom occupying a cluster consisting of two U vacancies and one O vacancy, which implies that diffusion occurs by a vacancy mechanism. The predicted diffusivity depends on the O non-stoichiometry of the fuel, which is governed by the prescribed O chemical potential. The latter may vary depending on the experimental setup, which has led to large variations in experimental data. In the calibration exercise presented in Sec. 3, an example will be provided of how the O chemical potential or partial pressure can be calculated for each experiment according to a self-consistent methodology.

2.2 Diffusivities under irradiation conditions: `Centipede` cluster dynamics simulations with input from density functional theory and empirical potentials calculations

The analytical point defect model applied for the thermal equilibrium case in Ref. [14] cannot be used under irradiation. Rather, the creation of point defects due to irradiation damage, their self-interaction and interaction with sinks must be modeled to capture the non-equilibrium response due to irradiation. This is accomplished by the `Centipede` cluster dynamics code originally developed under NEAMS and then continued to be developed under the NE-SciDAC project [18, 15]. The `Centipede` code and the underlying methodology was recently presented in Ref. [18] and applied to Xe diffusion in irradiated UO_2 in Ref. [15], as well as for related problems [28]. In short, `Centipede` solves a set of reaction equations that captures the creation of defects due to irradiation damage and their reactions with each other and lattice sinks. Each reaction is formulated in terms of the change in free energy, which governs the direction of the reaction and provides a natural way to account for O non-stoichiometry and other thermodynamic considerations. The reaction rate is influenced by the driving force, but even more so by the kinetic properties of the reacting defects. `Centipede` solves for the steady-state solution to the coupled set of reaction equations, which provides the concentration of point defects, clusters involving multiple point defects and clusters involving Xe atoms. Without the presence of irradiation, the solution to these equations reduces to that of the thermal equilibrium case. From the information on defect concentrations, diffusivities may be calculated by considering the concentration and mobility of each individual cluster. `Centipede` is implemented in the MOOSE framework [29].

The `Centipede` code focuses on accurately capturing the chemistry and irradiation response of point defects and relatively small defect clusters with up to about 10 U and 20 O vacancies interacting with a single Xe atom. This distinguishes it from the `Xolotl` cluster dynamics code used to simulate clusters of Xe atoms containing up to millions of atoms (gas bubbles). Unlike `Centipede`, `Xolotl` presently only accounts for Xe and does not explicitly track vacancies or interstitials in applications to UO_2. The small clusters targeted in the `Centipede` code are important for diffusion, while any cluster larger than roughly 10 U vacancies or containing more than one Xe atom acts as a small bubble rather than as a mobile cluster and consequently does not contribute much to diffusion. Instead it acts as a sink. `Xolotl` is currently being coupled to `Centipede` in order to resolve the full Xe-vacancy phase space in a single simulation.

Refs. [15] and [28] present the baseline results for U and Xe diffusion, respectively, which constitute the starting point for the sensitivity and uncertainty quantification exercises summarized in Sec. 3. The key results from the baseline cases are reproduced in Fig. 2. Although the prediction of U and Xe diffusivities are in fairly good agreement with available experimental data, the most accurate predictions required some by hand parameter calibration due to inherent uncertainties deriving from the underlying DFT and empirical potential calculations. Parameter uncertainty combined with model uncertainty results in predictions with a certain error bar, however the results in Fig. 2 give no indication of the magnitude of this error. This deficiency is addressed in the present study by estimating uncertainties for individual model parameters and performing a formal sensitivity and uncertainty quantification (UQ) analyses. The main new result of the present study is a demonstration of how the accuracy of model predictions can be improved by performing parameter calibration based on the experimental data reproduced in Fig. 2, while observing uncertainty ranges for the model parameters obtained from DFT and empirical potential calculations as well as uncertainties associated with the experimental data.

2.3 Intra-granular diffusion, bubble nucleation and growth simulated by the `Xolotl` code

The intra-granular fission gas behavior is modeled by the `Xolotl` cluster dynamics code, originally developed to simulate irradiated material in fusion reactors [20, 21, 22, 23, 24]. The current implementation assumes that all fission gas atoms are Xe. Moreover, UO_2 vacancies are not modeled and only Xe atoms and Xe clusters/bubbles are resolved. Vacancies and interstitials will be added in future work. `Xolotl` evolves the concentrations of clusters containing increasing numbers of Xe atoms. The evolution of each cluster size is determined by solving a PDE generally described as:

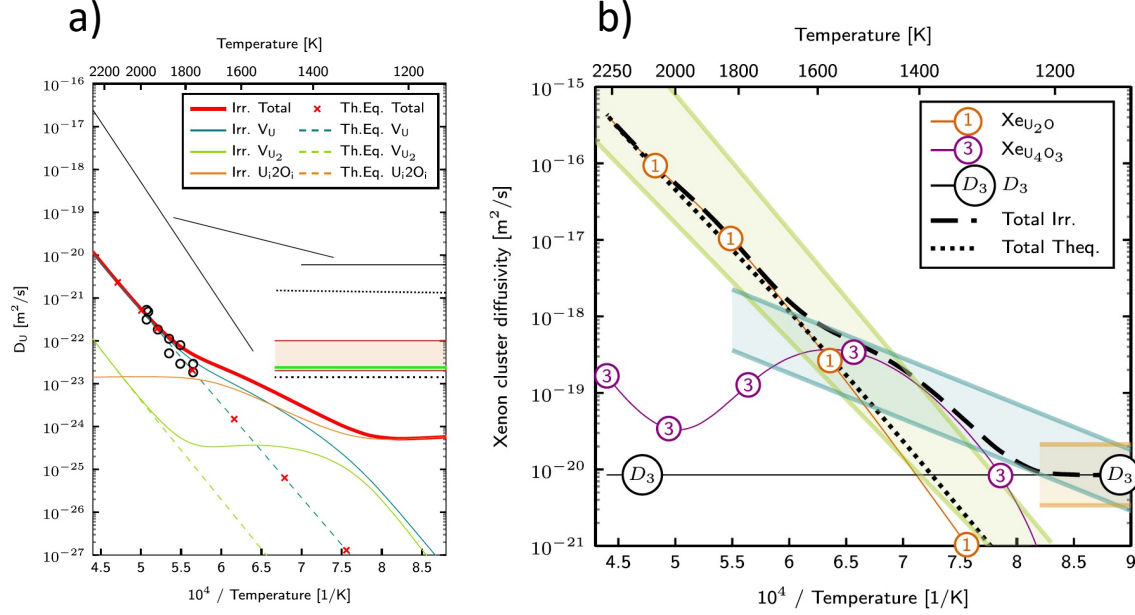$$\frac{\partial C_n}{\partial t} = \dot{F} y_n + D_n \Delta^2 C_n - Q(C_n), \tag{1}$$

Figure 2: Baseline `Centipede` predictions of U (a) and Xe diffusivities (b) in UO_2 compared to a subset of available experimental data [2, 1, 4], as reproduced from Refs. [18] and [15]. a) The solid red line refers to the total diffusivity under irradiation and the dashed blue line diffusion in thermal equilibrium. The circles refer to the most reliable experimental data. The solid black lines refer to experiments by Matzke. They deviate significantly from the predictions, which is presumed to be a consequence of sample oxidation. The other lines refer to contributions from individual diffusion mechanisms. (b) Xe diffusion coefficient as function of temperature in irradiated UO_2 predicted by the `Centipede` code are shown in black lines (long-dash line refers to the irradiation case and short-dash line to the thermal equilibrium case). The other lines represent the diffusivity due to the two main contributing clusters. Experimental data is shown as colored bands indicating the spread of data. The three different colors highlight the high (D_1), intermediate (D_2) and low (D_3) temperature diffusion regimes. In both figures, the legend defines the defect species contributing to diffusion using Kröger-Vink notation, see the original references for additional details.

10

where C_n is the concentration of a cluster containing n Xe atoms, the first right-hand-side term corresponds to the production of new Xe, the second term is the diffusion term, and the third term accounts for reactions between clusters. The Xe production is a function of the fission rate density $\dot{F}$ and the fission yield y_n of n Xe atoms per fission; fissions only yield single Xe atoms, such that $y_{n>1} = 0$. D_n is the diffusion coefficient of each Xe cluster, though only the smallest cluster is assumed to be mobile. The diffusivity of the mobile single Xe atom corresponds to the diffusivity calculated by `Centipede`. The last term in Eq. 3 represents the cluster reactions, which includes capture, emission and resolution of Xe atoms according to rates governed by either diffusion of single Xe atoms or resolution by fission fragments. The PDEs resulting from the cluster dynamics formulation are solved using the finite difference method (FDM) and implicit time integration with PETSc [23]. Further details of the `Xolotl` model and parameter values used in the simulations can be found in Ref. [30].

2.4 Inter-granular bubble evolution simulated by the `MARMOT` phase-field code

The phase-field method is a popular approach to model spatially-resolved microstructure evolution. Each phase or micro-structure feature is described by continuous variable fields that smoothly transition between values at interfaces, in our case grain boundaries or bubble surfaces, giving the interfaces a finite width. In addition to the non-conserved phase-field variables, conserved quantities such as concentration fields, are also tracked. Here, those correspond to the concentration of Xe and vacancies. The concentration variables are sometimes coupled to the phase-field variables, which is the case for the bubble phase in UO_2. The phase-field and concentration variables are evolved with time to minimize the free energy. In this work, the model from Aagesen et al. [31] that was developed to investigate the evolution of inter-granular gas bubbles in polycrystalline UO_2 was used. In this formulation the concentration fields are replaced with the chemical potential for improved numerical efficiency. Ref. [30] contains further details of the application of this methodology, including parameter values used in the simulations.

The system of partial differential equations obtained in the phase-field formulation are solved using the finite element method (FEM) with implicit time integration in the `MARMOT` mesoscale fuel performance code [27]. `MARMOT` is based on the Multiphysics Object-Oriented Simulation Environment (MOOSE) [29]], which uses the PETSc library [32] for solving the system of nonlinear equations. The computational cost of polycrystalline simulations is reduced by using the grain tracker system available in MOOSE [33].

2.5 Coupled `Xolotl`-`MARMOT` simulations of gas evolution and release

The intra-granular bubbles in UO_2 are only a few nanometers in diameter, which is very small compared to the size of grains and grain boundary bubbles. This makes it numerically

difficult to resolve all the disparate micro-structure features in irradiated UO_2 fuel using the phase-field method. Conversely, the cluster dynamics approach employed in `Xolotl` is challenging for very large bubbles due to the need to track a large set of cluster sizes and, moreover, this method does not explicitly represent the complex shape that bubbles at grain boundaries may take, which is desired for resolving the bubble evolution at grain boundaries and edges. For these reasons, a combined cluster dynamics and phase-field approach is pursued in the NE-SciDAC project. The `Xolotl` cluster dynamics code is used to describe the intra-granular bubbles and diffusion to grain boundaries and grain edges, while the `MARMOT` phase-field method is utilized for evolving grain boundary and edge bubbles as well as the grain micro-structure itself. The two codes are coupled by `Xolotl` providing the flux to grain boundaries as a source term in `MARMOT`, which then evolves grain boundaries and bubbles at grain boundaries. The grain micro-structure is returned to `Xolotl` by `MARMOT`. Details of the coupling strategy, including numerical performance, and simulation parameters for both `MARMOT` and `Xolotl` are available in Ref. [30]. Information transfer between the two codes is handled by the MultiApp and Transfer systems from the MOOSE framework [34].

2.6 Application of calculated diffusivities in reduced order fuel performance models (`Nyx`)

The models developed in the NE-SciDAC project targets implementation in the Bison fuel performance code. However, during the model development and testing phases, a stand-alone code called `Nyx`, developed by G. Pastore at UTK, is utilized. This code is focused on fission gas behavior only and does not attempt to solve the larger thermo-mechanical problem that is at the core of the capabilities in Bison.

More in detail, `Nyx` is an object-oriented C++ computer program designed to perform zero-dimensional (0D) "point" calculations. In other words, `Nyx` can be used to model fission gas behavior in a single location (comparable to a mesh point for an engineering fuel performance code), provided the local conditions as a function of the time (e.g., temperature and fission rate). While limited to a local analysis, `Nyx` provides the advantages of (i) a high computational efficiency (typically, a fraction of a second per calculation) and (ii) decoupling of the model of interest from the other aspects of fuel performance analysis. These characteristics facilitate and accelerate progress on model testing, sensitivity analysis, uncertainty quantification and validation. Models implemented in `Nyx` can be transferred to Bison once the development and testing phase is complete. This also provides additional confidence in the Bison application following prior consolidation of the models in the simpler `Nyx` framework.

`Nyx` incorporates an engineering model of intra-granular fission gas behavior previously developed in the NE-SciDAC project. The characteristics of the engineering model that are most relevant to the work presented here are briefly summarized below. More details are

given in previous NE-SciDAC milestone reports [35, 36] and in [26]. The model consists of the following system of coupled partial differential equations:

$$\frac{\partial N}{\partial t} = \nu - bN$$

$$\frac{\partial m}{\partial t} = 2\nu - bm + gc \tag{2}$$

$$\frac{\partial c}{\partial t} = yF + D\Delta^2 c - 2v + bm - gc,$$

where N (m^{-3}) is the number density of fission gas bubbles, m (m^{-3}) the concentration of gas atoms in bubbles, c (m^{-3}) the concentration of gas atoms in solid solution, ν (m^{-3}s^{-1}) the bubble nucleation rate, b (s^{-1}) the re-solution rate from bubbles, g (s^{-1}) the gas atom trapping rate at bubbles, y (/) the yield of fission gas atoms, F (m^{-3}s^{-1}) the fission rate and D (m^{2}s^{-1}) the gas atom diffusivity. D corresponds to the quantity calculated by `Centipede`. The average bubble radius is calculated as

$$R = \left(\frac{3\Omega}{4\pi n}\right)^{1/3}, \tag{3}$$

where Ω (m^3) is the atomic volume and n (-) the number of atoms per bubble. In this work, we use $y = 0.3$ and $\Omega = 4.09 \times 10^{-29}$ m^3, i.e., equal to the volume of the Schottky defect [37].

The object-oriented structure of `Nyx` makes it straightforward to extend the program to increasingly complex models and/or further physical phenomena.

3 `Centipede` uncertainty quantification and calibration

3.1 Calibration setup

We start with a high-level description of the calibration setup. Our goal is to calibrate a statistical model that approximates a set of physical quantities g_a, $a \in \mathcal{A}$, at a particular operating condition x. In the context of `Centipede`, the physical quantities g_a are the diffusivities, in particular U diffusivity under thermal equilibrium conditions (D_U^{eq}), Xe diffusivity under thermal equilibrium conditions (D_{Xe}^{eq}) and Xe diffusion under irradiation conditions (D_{Xe}^{irr}). The operating condition x is the temperature.

For each of the diffusivities, there is a corresponding data set

$$\mathcal{D}_a := \{x_a^{(n)}, y_a^{(n)}, s_a^{(n)}\}_{n=1}^{N_a},$$

which consists of N_a measurements $y_a^{(n)}$ that corresponds to the value of $g_a(x_a^{(n)})$, i.e., the value of the physical quantity g_a at operating condition $x_a^{(n)}$. For each nth measurement,

physical quantity	symbol	data set	#	reference
U diffusivity under thermal equilibrium	$D_{\mathrm{U}}^{\mathrm{eq}}$	Sabioni	10	[1]
Xe diffusivity under thermal equilibrium	$D_{\mathrm{Xe}}^{\mathrm{eq}}$	Davies & Long	10	[2]
Xe diffusion under irradiation	$D_{\mathrm{Xe}}^{\mathrm{irr}}$	Turnbull	16	[3, 4]

Table 1: Physical quantities (diffusivities) with their abbreviation, and corresponding data set and number of measurements (#) in each data set used in the calibration setup.

we also have a post-processed value $s_a^{(n)}$ for the measurement error associated with the measurement $y_a^{(n)}$. See Table 1 and Figure 3 for an overview of the different data sets. We use $\mathcal{D} := \{\mathcal{D}_a : a \in \mathcal{A}\}$ to denote the collection of all data sets.
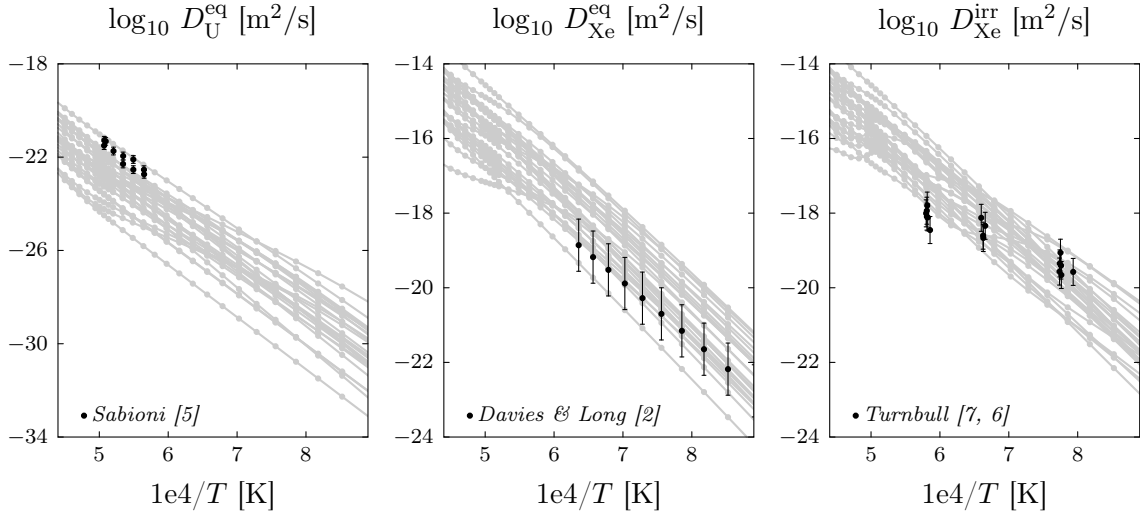

Figure 3: Samples of the different `Centipede` predictions for each diffusivity quantity and corresponding measurements.

The `Centipede` diffusivity predictions for a particular set of parameters $\boldsymbol{\nu}$ are given as a set of outputs $h_a^{(m)}(\boldsymbol{\nu})$ at particular operating conditions $x^{(m)}$, $m = 1, 2, \ldots, M$. We propose the model

$$g_a(x) = h_a(x; \boldsymbol{\nu}) + \varepsilon_a \tag{4}$$

where $\boldsymbol{\nu}$ is a set of calibrated parameter values, $h_a(x; \boldsymbol{\nu})$ is an interpolating function that agrees with the `Centipede` predictions $h_a^{(m)}(\boldsymbol{\nu})$ at the operating conditions $x^{(m)}$ and $\varepsilon \sim \mathcal{N}(0, \sigma_a^2)$ is a standard normal random variable with mean zero and unknown standard deviation σ_a. We consider equation (4) as an augmented probabilistic representation, where our goal is to calibrate both the model parameters $\boldsymbol{\nu}$ and the hyperparameters σ_a, $a \in \mathcal{A}$.

14

The goal is now to find the parameters $\boldsymbol{\zeta} := (\boldsymbol{\nu}, \sigma_{a_1}, \sigma_{a_2}, \ldots)$ that best match the statistics of the model $g_a(x_a^{(n)})$, evaluated at the operating conditions $x_a^{(n)}$, to the mean $y_a^{(n)}$ and standard deviations $s_a^{(n)}$ given in the data $\mathcal{D}_a$, for all measurements $n = 1, 2, \ldots, N_a$ and for all physical quantities $a \in \mathcal{A}$. We will resort to a Bayesian calibration setup to find the parameters $\boldsymbol{\zeta}$ given the available data $\mathcal{D}$. See Figure 4 for an overview of the calibration framework.
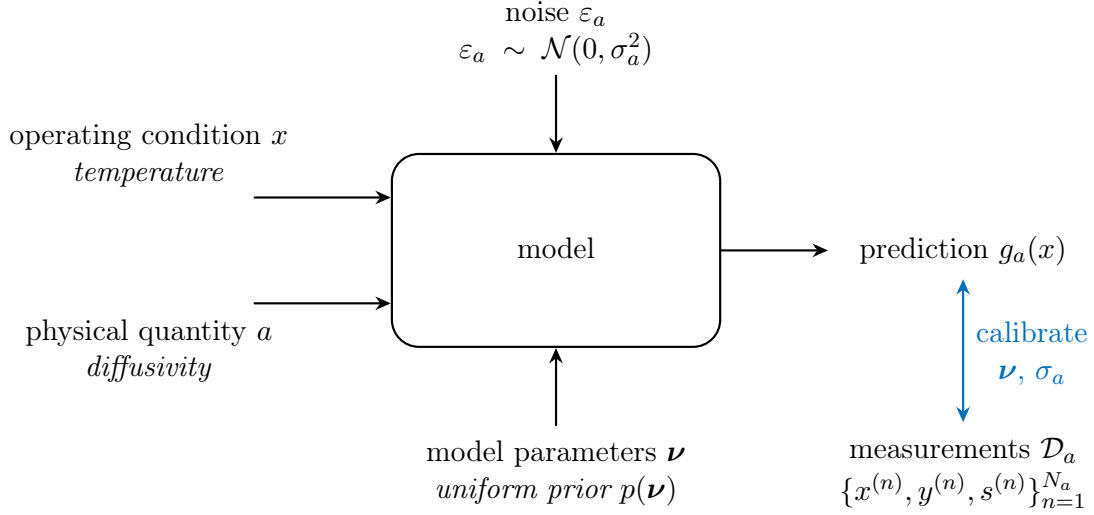

Figure 4: Schematic overview of the calibration problem.

In a Bayesian calibration setting, we require the posterior distribution $p(\boldsymbol{\zeta}|\mathcal{D})$, i.e., the distribution of the parameters given the data. The relationship between posterior $p(\boldsymbol{\zeta}|\mathcal{D})$ and prior $p(\boldsymbol{\zeta})$ is given by Bayes' law, i.e.,

$$p(\boldsymbol{\zeta}|\mathcal{D}) \propto \mathcal{L}(\boldsymbol{\zeta})p(\boldsymbol{\zeta}), \tag{5}$$

where $\mathcal{L}(\boldsymbol{\zeta})$ is the likelihood function for observing the data given the parameters $\boldsymbol{\zeta}$.

The calibration problem, as outlined above, where the goal is to match statistics of the model and the data, is particularly suited to be solved by *approximate Bayesian computation* (ABC). In particular, we propose the ABC likelihood

$$\mathcal{L}(\boldsymbol{\zeta}) \approx \mathcal{L}^{\mathrm{ABC}}(\boldsymbol{\zeta}) := \frac{1}{\sqrt{2\pi}\delta} \prod_{a \in \mathcal{A}} \prod_{n=1}^{N_a} \exp\left(-\frac{(h_a(x^{(n)}; \boldsymbol{\nu}) - y_a^{(n)})^2 + (\eta\sigma_a - s_a^{(n)})^2}{2\delta^2}\right), \tag{6}$$

where δ is a tolerance parameter. The likelihood function in (6) employs a Gaussian kernel whose argument is composed of the difference in mean and standard deviation of the model

15

and the data. In effect, the first term inside the exponential in equation (6) matches the mean of the model to the measurement $y_a^{(n)}$, while the second term matches the standard deviation of the model to the measurement error $s_a^{(n)}$. In the latter term, η is a scaling factor for the standard deviation to allow for different interpretations of the measurement error (i.e., 1σ, 2σ, ...).

It is in general impossible to compute the posterior $p(\boldsymbol{\zeta}|\mathcal{D})$ directly using equation (5). However, it is possible to generate samples from the posterior using Markov Chain Monte Carlo (MCMC). We resort to the adaptive MCMC implementation in `UQTk`, a collection of libraries and tools for the quantification of uncertainty in numerical model predictions, see [38, 39].

In the MCMC method, the likelihood function will typically be evaluated a large number of times. Since the expression in (6) contains a call to `Centipede`, i.e., $h_a(x^{(n)};\boldsymbol{\nu})$, the calibration setup quickly becomes computationally intractable. Therefore, we will replace the likelihood function $\mathcal{L}^{\text{ABC}}$ by an approximate likelihood function $\mathcal{L}^{\text{ABC}}_{\text{surrogate}}$ that uses a surrogate model instead of an actual call to `Centipede`. The surrogate model construction will be detailed in the next section.

3.2   Global sensitivity analysis and surrogate model construction

The calibration effort as outlined in Section 3.1 requires many `Centipede` model evaluations. To avoid excessive computational costs, we resort to a set of surrogate models that replace the expensive `Centipede` evaluations by a cheaper-to-evaluate alternative. To increase the accuracy of the surrogate models, we first perform a *global sensitivity analysis* (GSA) based on a first-order *polynomial chaos expansion* (PCE) surrogate model, to identify a subset of important parameters. Next, a higher-order PCE surrogate model is constructed using only the subset of important parameters.

A PCE surrogate model $f_a^{(n)}(\boldsymbol{\nu})$ for the `Centipede` prediction $h_a(x^{(n)})$ for physical quantity a at operating condition $x^{(n)}$ is defined as

$$f_a^{(n)}(\boldsymbol{\nu}) := \sum_{k=0}^{K-1} c_{a,k}^{(n)} \Phi_k(\boldsymbol{\xi}),$$

where $c_{a,k}^{(n)}$, $k = 0, 1, \ldots, K$ is a set of coefficients and $\Phi_k(\boldsymbol{\xi})$, $k = 0, 1, \ldots, K$ is a set of multivariate orthogonal polynomials expressed in terms of i.i.d. (Independent and identically distributed) random variables $\boldsymbol{\xi} := (\xi_1, \xi_2, \ldots, \xi_d)$. Since we assume a uniform distribution for the parameters ν_j, we have that $\xi_j \sim \mathcal{U}[-1, 1]$ for each $j = 1, 2, \ldots, d$, and the Φ_k are multivariate Legendre polynomials, see [40]. Furthermore, we assume that the input parameters ν_j can be written as a linear transformation of the random variables ξ_j for each

16

$j = 1, 2, \ldots, d$, i.e.,

$$\nu_j = \frac{\alpha_j + \beta_j}{2} + \frac{\beta_j - \alpha_j}{2} \xi_j$$

where α_j and β_j are the lower and upper bounds for the parameter ν_j, for each $j = 1, 2, \ldots, d$.

We initially rely on a first-order PCE model, that is,

$$f_a^{(n)}(\boldsymbol{\nu}) = \sum_{k=0}^{d} c_{a,k}^{(n)} \phi_k(\xi_k), \tag{7}$$

where ϕ_k, $k = 0, 1, \ldots d$, are univariate Legendre polynomials. The coefficients $c_{a,k}^{(n)}$ can be found by solving a regression problem using a set of input-output measurements. Given a PCE expansion as written in equation (7), it is easy to extract sensitivity indices. For example, the main-effect Sobol' indices $\mathfrak{s}_j^{(n)}$ can be computed as

$$\mathfrak{s}_j^{(n)} := \frac{(c_{a,j}^{(n)})^2 \langle \phi_k^2 \rangle}{\sum_{k=1}^{d} (c_{a,k}^{(n)})^2 \langle \phi_k^2 \rangle}.$$

The main effect indices $\mathfrak{s}_j^{(n)}$ allow for a natural way to order the parameters ν_j, $j = 1, 2, \ldots, d$, according to their importance.

We start by constructing a total of 3 (number of physical quantities in $\mathcal{A}$) $\times$ 26 (number of operating conditions M) first-order PCE surrogate models for the diffusivity predictions $g_a(x)$, $a \in \mathcal{A}$ at each temperature $x^{(m)}$, $m = 1, 2, \ldots, M$. The coefficients in the PCE expansion are determined by solving a least-squares regression problem with 10,000 `Centipede` runs.

For each surrogate model, we compute the main-effect Sobol' indices $\mathfrak{s}_j^{(n)}$, $j = 1, 2, \ldots, d$, see Figure 5. Next, we select the top 5 most important parameters for each diffusivity quantity. This results in a set of 9 important parameters (some of them are common between the sets), see Table 2.

Finally, we construct a set of third-order accurate PCE surrogate models using this subset of 9 important parameters. The third-order construction was determined to be a good trade-off between accuracy and overfitting. See Figure 6 for a visual comparison of the accuracy of the first-order 183-dimensional and third-order 9-dimensional PCE surrogate models.

The use of these surrogate model effectively lowers the computational burden of the calibration setup in the next section. One single evaluation of Centipede, computing the diffusivities for all 26 temperatures $x^{(m)}$, takes roughly 10 minutes, while evaluating the polynomial surrogate model is almost instantly (in the order of milliseconds on our current hardware).
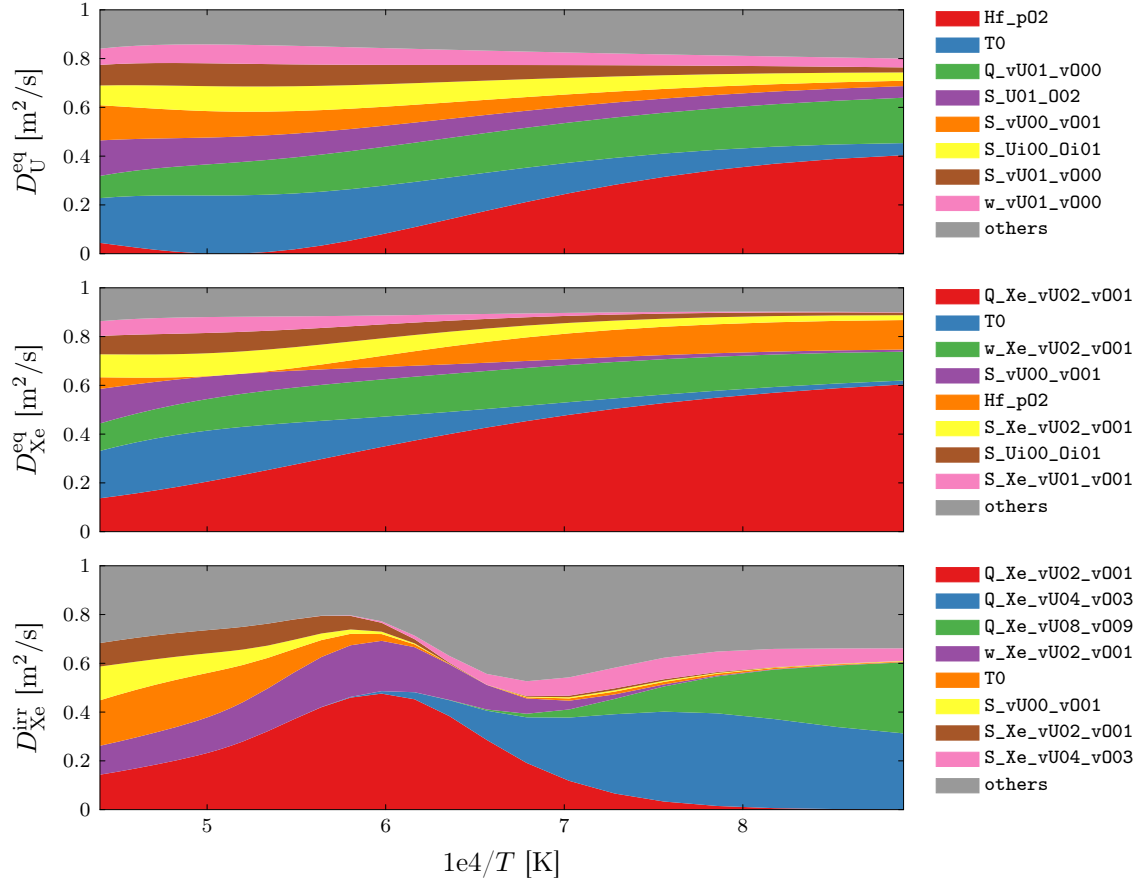
17

Figure 5: Evolution of the main-effect sensitivity indices for all 183 parameters as a function of temperature for all three diffusivities. The top 5 most important parameters for each diffusivity quantity are joined to form the reduced set of parameters. `Q` parameters refer to activation energies for diffusion, `w` parameters to attempt frequencies, `S` parameters to defect formation or binding entropies, `T0` to the temperature at which UO_2 is perfectly stoichiometric at given chemical conditions and `Hf_pO2` to the temperature dependence of the O partial pressure. The subscripts denote the number of U and O point defects that make up each cluster. See Refs. [18] and [15] for further explanations.
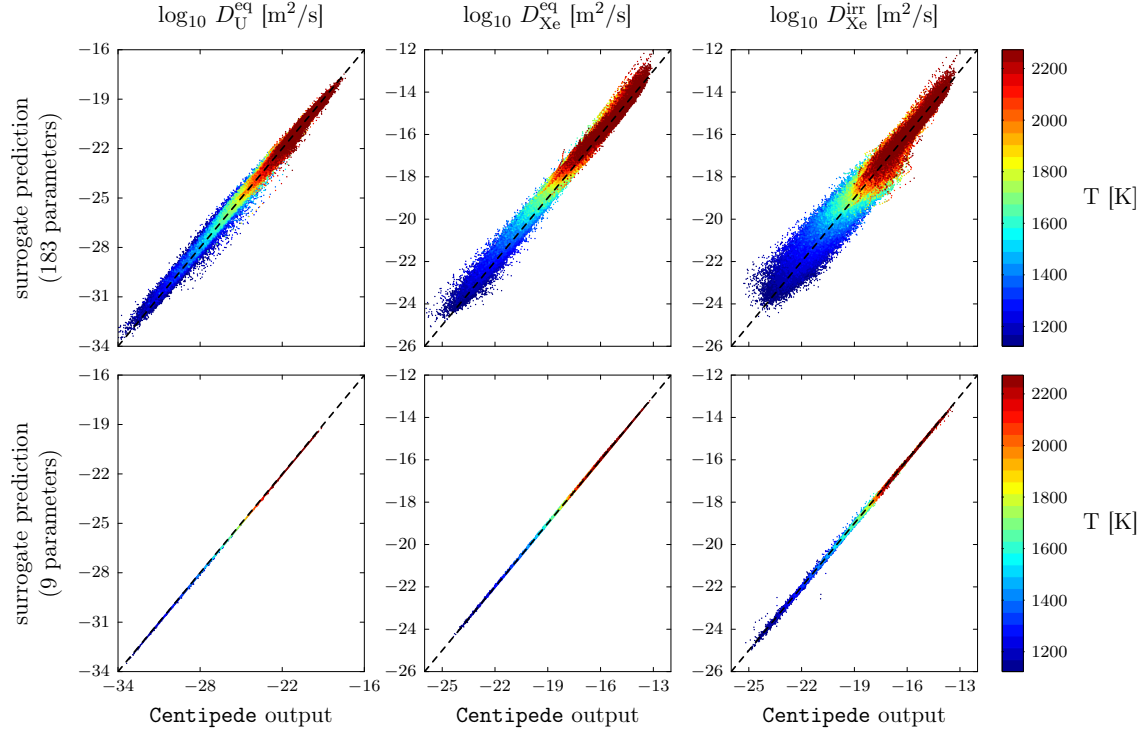
Figure 6: Comparison of `Centipede` output and polynomial surrogate output for all three diffusivities (*top row*: 183-parameter case, *bottom row*: 9-parameter case). The black dashed line indicates an identity relation. Because the regression problem that needs to be solved in order to compute the polynomial chaos coefficients is much harder to solve in 183 dimensions, the resulting surrogate predictions are less accurate for the 183-parameter case (*top row*).

3.3 Bayesian calibration of `Centipede`

With the surrogate models from Section 3.2 available, the call to `Centipede`, i.e., $h_a(x^{(n)}; \boldsymbol{\nu})$ in (6), is replaced by a call to the third-order PCE surrogate model $f_a^{(n)}(\boldsymbol{\nu})$, which results in the final likelihood

$$\mathcal{L}^{\mathrm{ABC}}(\boldsymbol{\zeta}) \approx \mathcal{L}^{\mathrm{ABC}}_{\mathrm{surrogate}}(\boldsymbol{\zeta}) := \frac{1}{\sqrt{2\pi}\delta} \prod_{a \in \mathcal{A}} \prod_{n=1}^{N_a} \exp\left(-\frac{(f_a^{(n)}(\boldsymbol{\nu}) - y_a^{(n)})^2 + (\eta\sigma_a - s_a^{(n)})^2}{2\delta^2} \right).$$

Next, we use MCMC to get samples from the desired posterior $p(\boldsymbol{\zeta}|\mathcal{D})$, see Section 3.1. To find good starting values for the Markov chain, we prepend the MCMC sampling with a few iterations of L-BFGS. Furthermore, to ensure that $\sigma_a \geq 0$ for all $a \in \mathcal{A}$ (σ_a can be interpreted as a standard deviation and should be non-negative), we infer $\mu_a := \log(\sigma_a)$ instead for each $a \in \mathcal{A}$. Finally, we use a tolerance $\delta = 0.1$, a proposal jump size of 0.25, set $\eta = 1$ and perform 100,000 MCMC iterations.

The reduced set of parameters identified during the GSA study in Section 3.2 contains two parameters, `T0` and `Hf_pO2`, that correspond to experimental or operating conditions that may in principle be different for each data set. Thus, we consider two different cases:

- a "**single**" case where we infer a single value of `T0` and `Hf_pO2` irrespective of the data set, and

- a "**multiple**" case where we infer multiple values of `T0` and `Hf_pO2`, one for each data set.

The latter case is implemented by extending the set of parameters to calibrate with additional parameters that are data-set specific (`T0`, `Hf_pO2`) pairs, in the sense that the first data set will only impact the first (`T0`, `Hf_pO2`) pair, the second data set will only impact the second (`T0`, `Hf_pO2`) pair and similar for the third data set. See Table 2 for an overview of these parameters.

In Figure 7, we compare the 5%, 10%, ..., 95% quantiles of the push-forward prior, i.e., the predictions of the diffusivities assuming the prior parameter ranges, and the posterior predictive, i.e., the predictions of the diffusivities assuming the posterior parameter distributions in the model from equation (4), for both the "single" and the "multiple" case. In Figure 8, we compare the diffusivities predicted using the *maximum a posteriori* (MAP) parameters, i.e., the most likely parameters, for both the surrogate model and `Centipede`. The surrogate prediction and the `Centipede` prediction are in reasonable agreement. Also shown on the figure is the `Centipede` prediction using the nominal, uncalibrated parameter values. We note in particular the discrepancy between the "single" and the "multiple" case for Xe diffusivity under thermal equilibrium conditions. The latter features a different mechanism at work at high temperatures, which is caused by more reducing conditions as determined by the much lower `T0` value for this case.

parameter name	lower bound	upper bound	nominal value	calibrated value	
				"single"	"multiple"
S_U01_O02	−129370.08	−129367.58	−129368.83	−129369.97	−129369.72
S_vU00_v001	−129287.92	−129285.42	−129286.67	−129287.88	−129287.87
Q_vU01_v000	3.98	4.48	4.23	4.09	4.00
Q_Xe_vU02_v001	3.45	3.95	3.70	3.70	3.68
Q_Xe_vU04_v003	2.52	3.02	2.77	2.52	2.54
Q_Xe_vU08_v009	2.88	3.38	3.13	2.89	2.89
w_Xe_vU02_v001	1.62	32.50	3.25	1.70	1.72
T0 (U diffusion)	1773.00	2173.00	1973.00	2157.46	2166.53
Hf_pO2 (U diffusion)	3.85	6.35	5.10	5.56	5.99
T0 (Xe diffusion)	1773.00	2173.00	1973.00	2157.46	1809.43
Hf_pO2 (Xe diffusion)	3.85	6.35	5.10	5.56	4.21
T0 (Xe irradiation)	1773.00	2173.00	1973.00	2157.46	1777.46
Hf_pO2 (Xe irradiation)	3.85	6.35	5.10	5.56	5.09

Table 2: Lower bound, upper bound, nominal value (from original uncalibrated parameter set), calibrated value for the "single" case and calibrated value for the "multiple" case for the set of important parameters in `Centipede`. The last 6 rows correspond to 3 (number of data sets) × 2 (number of operating conditions) copies of `T0` and `Hf_pO2` that we calibrate only in the "multiple" case. For the "single" case, the last 4 rows are just duplicates of rows 8 and 9. See 5 for explanation of parameter labels.

Fig. 9 plots the `Centipede` output for Xe diffusivity under irradiation conditions (both "single" and "multiple" cases), the Davies & Long data set for Xe diffusivity under thermal equilibrium conditions, the Turnbull data set for Xe under irradiation conditions, as well as the Turnbull correlation from [3]. Note that the athermal D_3 term contributing to diffusion below about 1200 K is not included in this plot. The two calibrated curves and the Turnbull correlation agree well between each other below 2000 K and also with the experimental data due to Turnbull used for the model calibration. The `Centipede` predictions also agree very well with the extrapolation of the Davies & Long data to high temperatures, which is a positive outcome since those diffusivities have been shown to work well in a number of macro-scale fuel performance assessments. In fact, this is an interesting observation for the case with multiple `T0` and `Hf_pO2` values, since the irradiation case values for these parameters, which were used in Fig. 9, are noticeably different from those obtained from the Davies & Long data (see Table 2). The good agreement with the extrapolated Davies & Long data for the irradiation case parameter set is obtained due to Xe interstitials emerging as the dominant diffusion mechanism above 1800 K. The emergence of the Xe interstitial mechanism for the multiple `T0` and `Hf_pO2` parameter set is a consequence of the conditions being more reducing, which in turn is a result of the much lower `T0` value obtained for this case. In the case of single `T0` and `Hf_pO2` values, the vacancy mechanism remains dominant at high temperature. Additional work is still needed to analyze the calibrated values for the different cases and to determine which set is the most appropriate, which will include extending the Davies & Long correlation to higher temperatures as well as assessing `Centipede` predictions against thermodynamic data on UO_2 non-stoichiometry. Even though the different correlations agree well in much of the temperature range, the differences at high temperature could impact simulations for certain accident scenarios. Differences would also emerge if the prevalent chemistry conditions of the fuel changed as a consequence of, for example, doping [28].

4 Uncertainty propagation in `Nyx`

Having calibrated the `Centipede` model parameters to experimental data using the sensitivity analysis and surrogate machinery described previously, it is straightforward to make predictions of Xe diffusivity with uncertainty by sampling the posterior parameter distribution and pushing these samples through the data model using the surrogates. For the remainder of this section, we use the calibrated diffusivities from the "multiple" case from Section 3.3. The Xe diffusivities can also be easily evaluated at arbitrary temperatures through interpolation between the temperatures at which the individual surrogates were constructed, such as in Fig. 7 where the surrogates were constructed to span a temperature range corresponding to three different experiments. We are interested in propagating the uncertainty in the Xe diffusivity in particular through higher-level models relevant to the prediction of intra-granular fission bubble formation. We employ the `Nyx` code to make
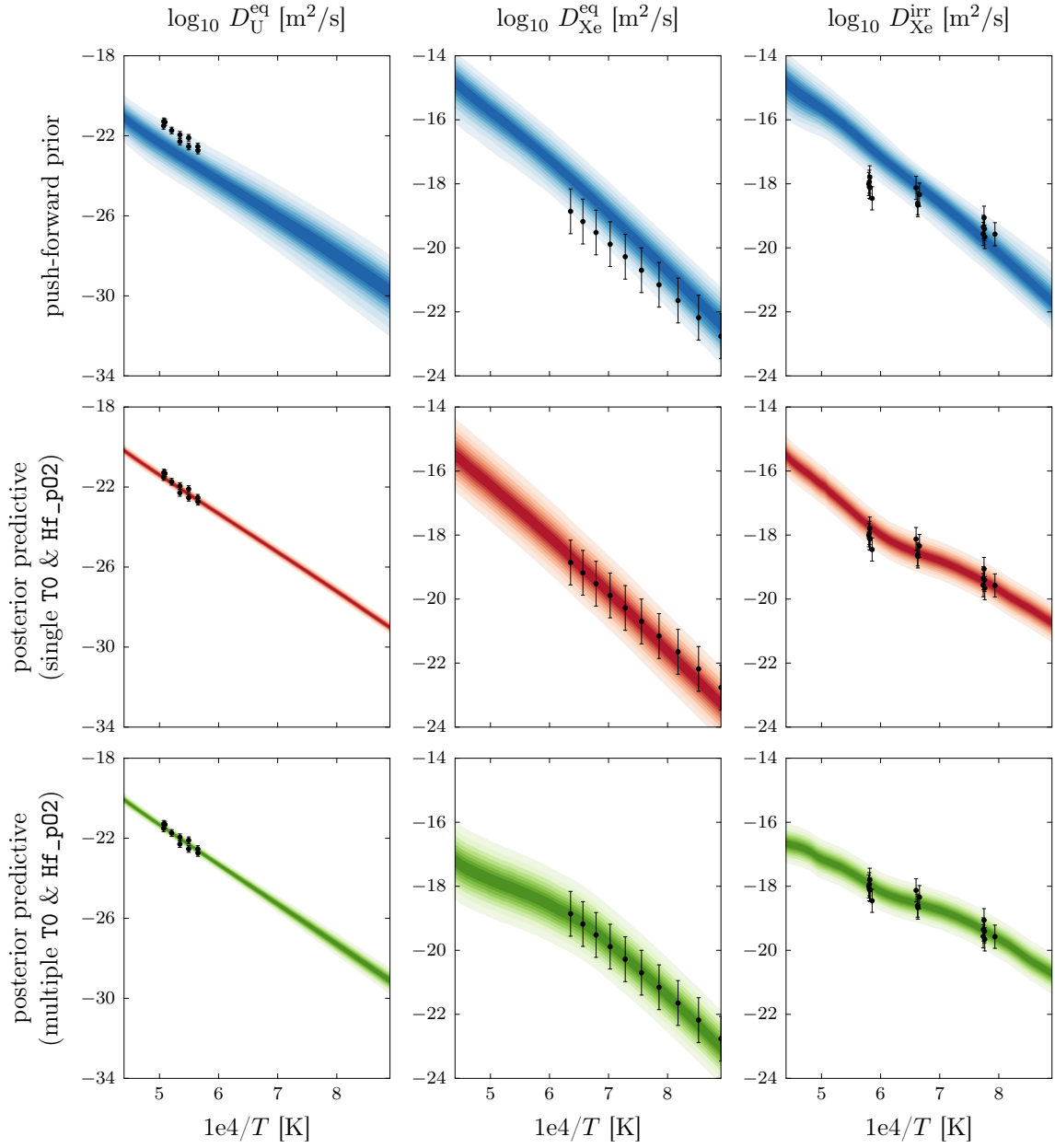
Figure 7: 5%, 10%, ..., 95% uncertainty quantiles of push-forward prior (*top row*), posterior predictive with a single value of `T0` and `Hf_pO2` (*middle row*), posterior predictive with multiple values of `T0` and `Hf_pO2`, one for each data set (*bottom row*).
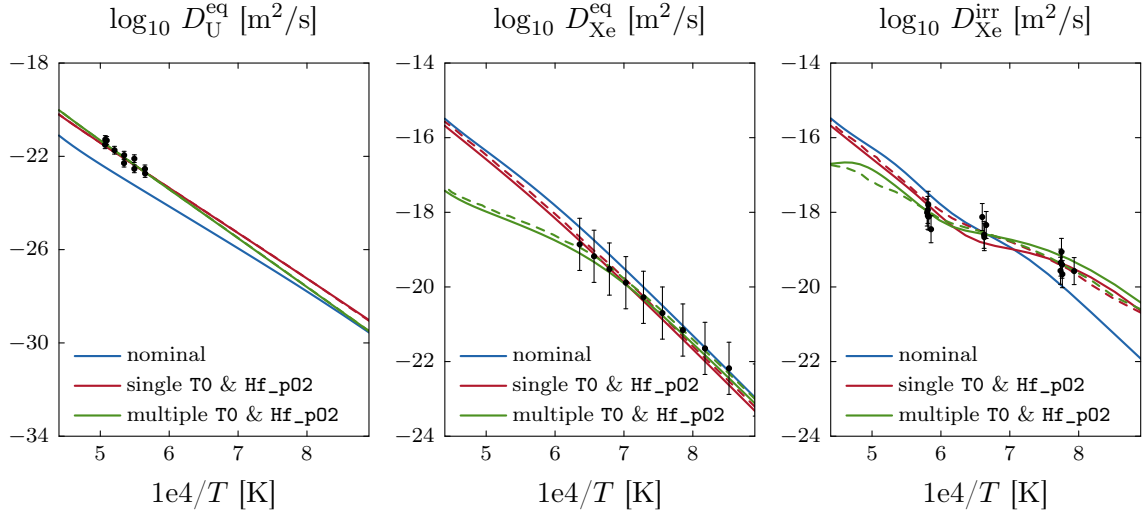
Figure 8: Comparison of the `Centipede` prediction with the nominal parameter values (original uncalibrated parameters), the prediction of the surrogate model using the MAP parameters (*dashed line*, ---) and the `Centipede` prediction using the MAP parameters (*full line*, ——) with a single value of `T0` & `Hf_pO2` and multiple values of `T0` & `Hf_pO2`, one for each data set.
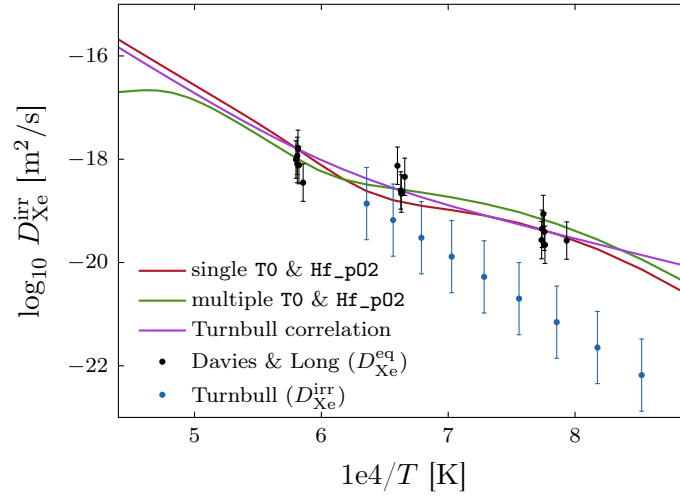

Figure 9: `Centipede` output for Xe diffusivity under irradiation conditions (both "single" and "multiple" cases), the Davies & Long data set for Xe diffusivity under thermal equilibrium conditions, the Turnbull data set for Xe under irradiation conditions, as well as the Turnbull correlation from [3].

predictions of quantities associated with bubble formation at conditions specified by the experiments of Baker [5], in order to compare to available experimental bubble data from White & Tucker [41].

Using 5000 samples of the uncertain diffusivities, `Nyx` simulations were performed to predict the bubble number density, atoms per bubble, and bubble radius at temperatures of 1573, 1673, and 1773 K respectively (see Figures 10 to 12). A general trend in the predictions is the decrease in uncertainty in the quantities with increasing temperature, and improved agreement of the mean predictions and those using the nominal inputs from the Turnbull correlation. This improved agreement can be attributed to the agreement between the Turnbull correlation and the diffusivity samples at higher temperatures (Figure 13).

When comparing to the available experimental data in the case of bubble number density (Figure 10), the `Nyx` predictions are consistently lower than the experimental data, even when taking into account the uncertainty in diffusivity. For predictions of bubble radius the predictions are consistently higher (Figure 12), and the experimental data points lie close to the lower bound of the 95% interval. Nevertheless, it is apparent that uncertainty in Xe diffusivity alone is not able to explain the discrepancy between the data and model predictions. As such it is important to consider additional sources of uncertainty that affect the simulation predictions. Figure 14 shows `Nyx` predictions at 1573 K of the three quantities of interest where uncertainty in the intra-granular resolution rate has also been accounted for in the simulations. A scaling factor of $1/\sqrt{10}$ is assigned to the nominal resolution rate (i.e. allowing the resolution rate to vary by a factor of 10 from its lower to upper bound). With this added source of uncertainty the experimental data is now enveloped by the `Nyx` predictions, where the variation in resolution rate has a strong effect on the predicted bubble number density in particular.

5   `Xolotl`-`MARMOT` simulations using uncertainty quantified and calibrated Xe diffusivity

Two dimensional, coupled `Xolotl` and `MARMOT` simulations have been performed to assess the impact of the UQ-based calibrated Xe diffusivity presented in this report, using either the one or multiple `Hf_pO2` and `T0` parameter sets. Note that for each simulation or experiment, there is only one set of `Hf_pO2` and `T0` values, but for the multiple case those values were derived by allowing each experiment to have a unique set. The coupled cluster dynamics and phase field simulations were performed at a temperature of 1400 and 1800 K, respectively, and included Xe clustering and bubble formation within grain interiors and fission fragment induced partial resolution of the fission gas bubbles with a size dependence as framed by Setyawan and co-workers [19]. The 2D simulations had a spatial domain of 20 μm by 20 μm, and included 5 grains with an initial 14 grain boundary bubbles. The spatial mesh was 125 by 125, and 3 different simulations were performed at each temperature, in order to
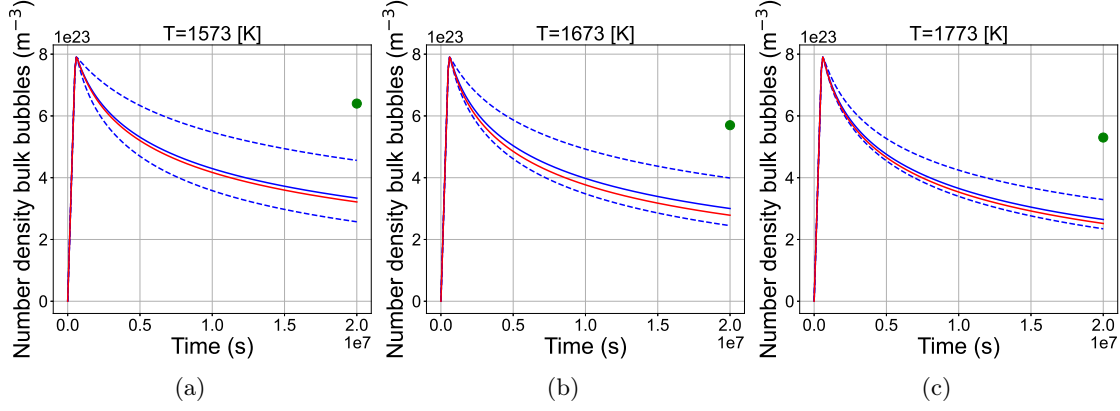
Figure 10: Time-evolving number density of bulk bubbles at (a) 1573 K, (b) 1673 K, and (c) 1773 K. The solid red lines indicate `Nyx` solutions using nominal diffusivity values from the correlation of Turnbull [3], i.e. without uncertainty. The solid blue line is the mean prediction when propagating the uncertain diffusivity following Bayesian calibration, with the dashed lines indicating the envelope of the 95% interval of the predictions. The green circle at 2.0×10^7 s is experimental data [41].
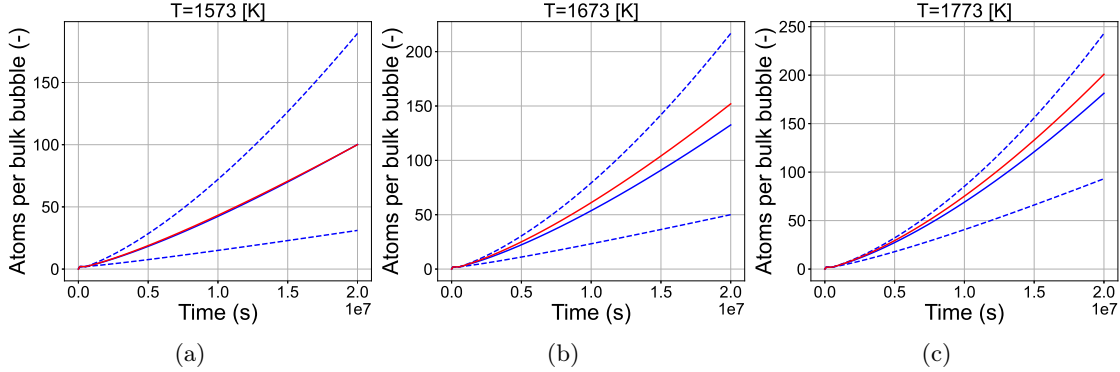

Figure 11: Time-evolving atoms per bulk bubble at (a) 1573 K, (b) 1673 K, and (c) 1773 K. The solid red lines indicate `Nyx` solutions using nominal diffusivity values from the correlation of Turnbull [3], i.e. without uncertainty. The solid blue line is the mean prediction when propagating the uncertain diffusivity following Bayesian calibration, with the dashed lines indicating the envelope of the 95% interval of the predictions.

compare the differences with Xe diffusion coefficient between the Turnbull expression [3], as well as the one and multiple parameter `Hf_pO2` and `T0` fits from the UQ assessment and calibration. The Xe diffusivity values used in these simulations are provided in Table 3.
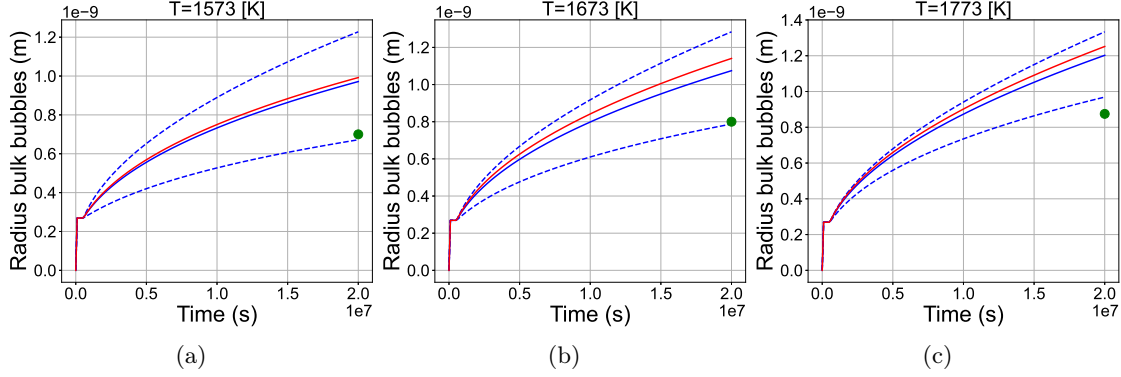
Figure 12: Time-evolving bubble radius at (a) 1573 K, (b) 1673 K, and (c) 1773 K. The solid red lines indicate `Nyx` solutions using nominal diffusivity values from the correlation of Turnbull [3], i.e. without uncertainty. The solid blue line is the mean prediction when propagating the uncertain diffusivity following Bayesian calibration, with the dashed lines indicating the envelope of the 95% interval of the predictions. The green circle at 2.0×10^7 s is experimental data from [41].
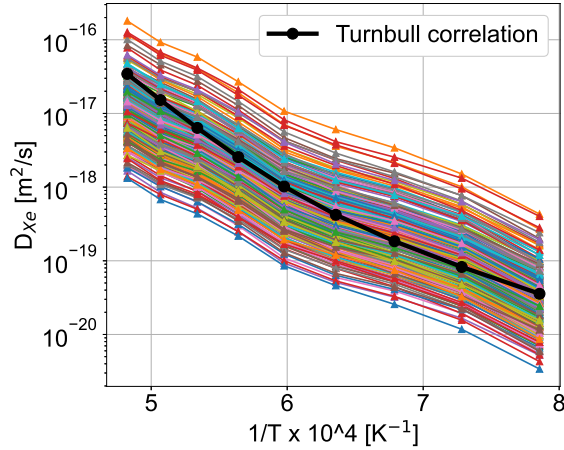

Figure 13: Diffusivity samples from the calibrated model compared to the correlation of Turnbull [3] across temperatures

Fig. 15 plots the results of these simulations, in which the Xe monomer concentration within the grains is plotted in Fig. 15a (1400 K) and Fig. 15c (1800 K), and the inter-granular fission gas bubble volume fraction (porosity) is plotted in Fig. 15b (1400 K) and Fig. 15d (1800 K). As expected, the higher irradiation temperature results in lower intra-granular Xe concentration and more Xe transport to the grain boundary bubbles, resulting in slightly
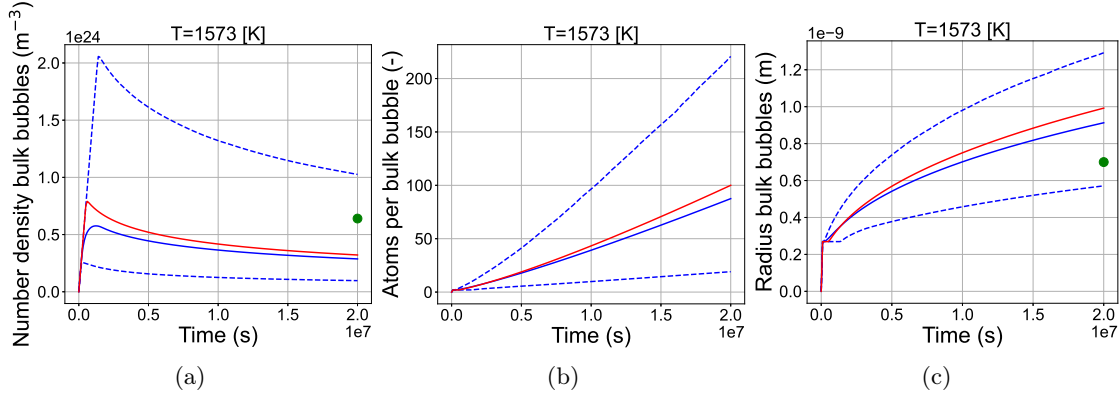
27

Figure 14: Time-evolving number density of bulk bubbles (a), time-evolving atoms per bulk bubble (b) and time-evolving bubble radius (c) at 1573 K, with additional uncertainty in the intra-granular resolution rate. The solid red lines indicate `Nyx` solutions using nominal diffusivity values from the correlation of Turnbull [3], i.e. without uncertainty. The solid blue line is the mean prediction when propagating the uncertain diffusivity following Bayesian calibration, with the dashed lines indicating the envelope of the 95% interval of the predictions. The green circle at 2.0×10^7 s is experimental data [41].

	Turnbull [3]	Single `Hf_pO2` and `T0`	Multiple `Hf_pO2` and `T0`
1400 K	0.091	0.103	0.183
1800 K	3.04	5.21	3.14

Table 3: Temperature and Xe diffusivity (in nm^2s^{-1}) used in 2D, coupled Xolotl and Marmot simulations. Single and Multiple `Hf_pO2` and `T0` refer to the one vs multiple `Hf_pO2` and `T0` parameter sets.

larger porosity relative to the lower temperature of 1400 K. Notably, the modification of the Xe diffusivity does not change the qualitative evolution of the monomer Xe concentration nor the predicted porosity, although there are some relatively minor quantitative differences. As shown in Table 3 and Fig. 15, the single parameter calibrated Xe diffusivity agrees better with that predicted by Turnbull [3] at 1400 K, whereas the multi parameter (multi) calibrated diffusivity agrees better with the Turnbull prediction at 1800 K. Future effort will further analyze the impact of the newly calibrated Xe diffusion models against a variety of experimental data.

In addition, the diffusion values from Turnbull and those from the calibrated Centipede simulation results were compared in a stand-alone phase-field model of fission gas release using the `MARMOT` code [27] (no coupling to `Xolotl`). In the simulation, fission gas was
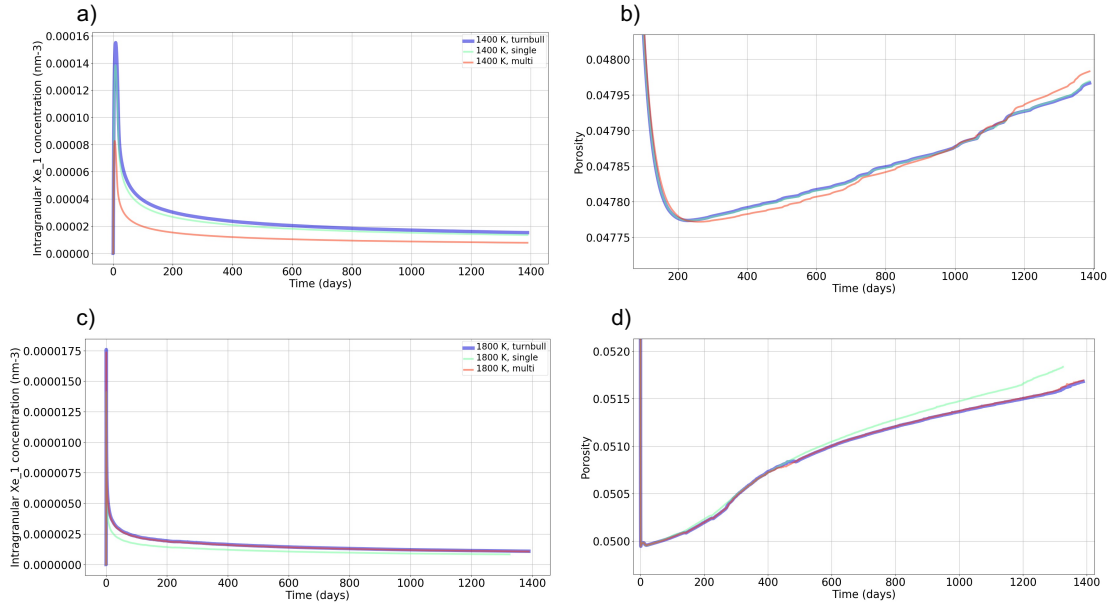
Figure 15: Predicted Xe monomer concentration {a) and c)} and inter-granular bubble volume fraction (porosity) {b) and d)} from 2D coupled `Xolotl-MARMOT` modeling at 1400 {a) and b)} versus 1800 K {c) and d)}.

produced within a 30 μm$\times$30 μm 2D polycrystal of UO$_2$. It had 36 initial grains, with an average grain size of 5 μm, and 20 initial intergranular fission gas bubbles, as shown in Fig. 16a. The left side of the domain was a free surface, such that gas that reached it was released. The fission gas behavior was simulated over 260 days at 1200 K with a fission rate of 1.09×10^{13} fissions/(cm^{3}s). As can be seen in Fig. 16b, the simulations using the Turnbull and Centipede diffusion coefficients resulted in nearly identical amounts of gas released over time, which is no surprise given the similarity of the two diffusion coefficients at 1200 K. Future work will explore cases where the models are expected to perform differently, as previously discussed.
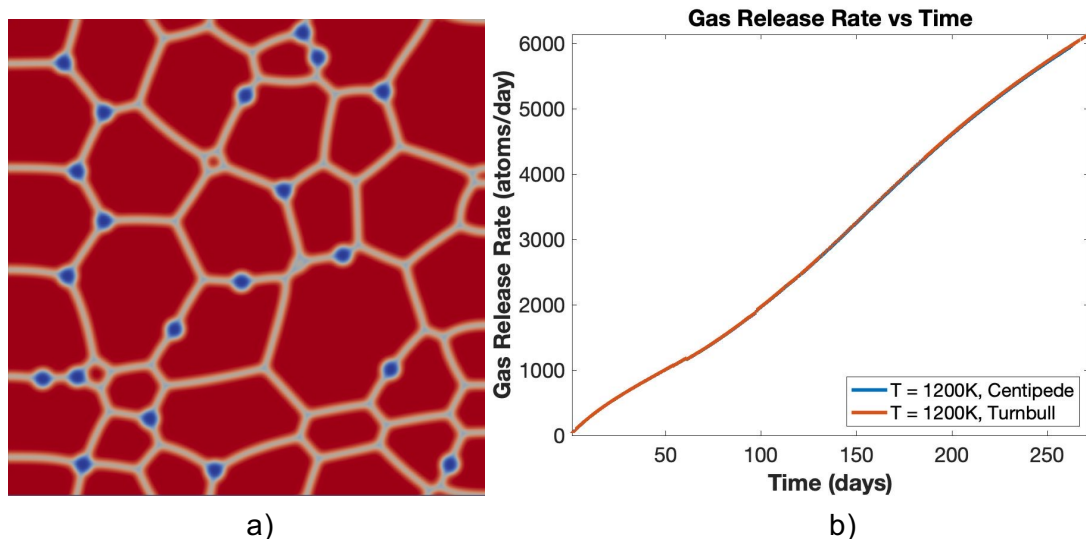

Figure 16: Comparison of the fission gas release predicted by MARMOT using the Turnbull and `Centipede` diffusion coefficients. (a) Initial microstructure used in the fission gas phase field simulations, where the left side is a free surface; (b) Plot of the gas release rate from the left side of the domain predicted using the two diffusion coefficient values.

6   Conclusions

The `Centipede` code predicts the diffusion rate of fission gas atoms (Xe) in irradiated UO$_2$ nuclear fuel by solving a set of rate equations describing the response of point defects, defect clusters as well as their interaction with Xe to irradiation. The model contains 183 parameters that were previously determined from atomic-scale simulations. The Xe diffusivities predicted by the model were in reasonable agreement with experiments, however, given the complexity of the model, uncertainties may be significant and consistency with experimental data may not be complete. In the present study, a statistical model based

on `Centipede` was calibrated that predicts both the value of the Xe diffusivity in good agreement with available data and the uncertainty associated with the prediction. The model parameters were refined using Bayesian calibration with a dedicated *approximate Bayesian computation* (ABC) likelihood function. To avoid excessive computational costs, the expensive `Centipede` simulation code was replaced by a higher-order surrogate model, constructed using only the 9 most important parameters. These important parameters were identified by a preliminary *global sensitivity analysis* (GSA) study. Two different strategies were employed in the calibration. The first considers the chemistry in all experiments to be the same regardless of the conditions and the second instead ascribes unique chemistry to each experimental measurement, which is considered to be the more accurate representation of the experimental conditions. The chemistry controls the O non-stoichiometry, which impacts the concentration of point defects, defect clusters and consequently diffusion. Both calibration sets achieve good agreement with experimental data, but nevertheless show distinct features related to the defect chemistry at high temperature. Those will be further investigated in future work.

Finally, the diffusivity predictions by `Centipede` are used as input to to engineering scale simulations using the `Nyx` code (reduced order fuel performance code focused on gas behavior alone) and meso-scale simulations of the intra- and inter-granular fission bubble evolution using the coupled `Xolotl-MARMOT` code. The `Nyx` simulations included uncertainty propagation and the results were used to estimate quantities associated with inter-granular bubble formation at conditions specified by the experiments of [5]. The uncertainty of the Xe diffusion coefficient was not sufficient to bound all the experimental data, but adding uncertainties for the intra-granular bubble resolution rate results in the experimental data points being bound by the envelope of the 95% interval of the predictions. The `Xolotl-MARMOT` simulations were compared to simulations using the baseline diffusivities from Turnbull et al. [3]. Overall, since the calibrated `Centipede` prediction of diffusivities are close to the Turnbull model, the `Xolotl-MARMOT` simulations based on the two models are similar. However, since the Turnbull model does not incorporate any sensitivity to chemistry, it will always predict the same gas evolution regardless of fuel composition, while the mechanistic `Centipede` model is able to capture those changes and, moreover, the calibrated predictions will contribute to capturing those changes with higher accuracy as compared to the nominal parameter values.

Future work will add thermodynamic data on $UO_{2\pm x}$ non-stoichiometry to the data set used for parameter calibration.

References

[1] A. C. S. Sabioni, W. B. Ferraz, F. Millot, First study of uranium self-diffusion in UO_2 by sims, J. Nucl. Mater. 257 (1998) 180–184.

[2] D. Davies, G. Long, The emission of Xe-133 from lightly irradiated uranium dioxide spheroids and powders, Tech. rep., United Kingdom Atomic Energy Authority. Research Group. Atomic Energy Research Establishment, Harwell, Berks, England (United Kingdom) (1963).

[3] J. Turnbull, C. Friskney, J. Findlay, F. Johnson, A. Walter, The diffusion coefficients of gaseous and volatile species during the irradiation of uranium dioxide, J. Nucl. Mater. 107 (1982) 168–184.

[4] J. Turnbull, R. White, C. Wise, The diffusion coefficient for fission gas atoms in uranium dioxide, Tech. rep., International Atomic Energy Agency (IAEA), Vienna (Austria) (1989).

[5] C. Baker, The fission gas bubble distribution in uranium dioxide from high temperature irradiated sghwr fuel pins, J. Nucl. Mater. 66 (1977) 283–291.

[6] A. Booth, A method of calculating gas diffusion from UO_2 fuel and its application to the x-2-f test, Tech. rep., Atomic Energy of Canada Limited (1957).

[7] M. V. Speight, A calculation on the migration of fission gas in material exhibiting precipitation and re-solution of gas atoms under irradiation, Nucl. Sci. Eng. 37 (1969) 180.

[8] R. M. Cornell, M. V. Speight, B. C. Masters, A calculation on the migration of fission gas in material exhibiting precipitation and re-solution of gas atoms under irradiation, J. Nucl. Mater. 30 (1969) 170.

[9] J. A. Turnbull, C. A. Friskney, J. R. Findlay, F. A. Johnson, A. J. Walter, The diffusion coefficients of gaseous and volatile species during the irradiation of uranium dioxide, J. Nucl. Mater. 107 (1982) 168.

[10] R. J. White, M. O. Tucker, A new fission-gas release model, J. Nucl. Mater. 118 (1983) 1.

[11] K. Forsberg, A. R. Massih, Fission gas release under time-varying conditions, J. Nucl. Mater. 127 (1985) 141.

[12] A. R. Massih, K. Forsberg, Calculation of grain boundary gaseous swelling in UO_2, J. Nucl. Mater. 377 (2008) 406.

[13] G. Pastore, L. Luzzi, V. Di Marcello, P. Van Uffelen, Physics-based modelling of fission gas swelling and release in UO_2 applied to integral fuel rod analysis, J. Nucl. Mater. 256 (2013) 75.

[14] R. Perriot, C. Matthews, M. W. Cooper, B. P. Uberuaga, C. R. Stanek, D. A. Andersson, Atomistic modeling of out-of-pile xenon diffusion by vacancy clusters in UO_2, J. Nucl. Mater. 520 (2019) 96–109.

[15] C. Matthews, R. Perriot, M. Cooper, C. R. Stanek, D. A. Andersson, Cluster dynamics simulation of xenon diffusion during irradiation in UO_2, Journal of Nuclear Materials 540 (2020) 152326.

[16] D. Andersson, P. Garcia, X.-Y. Liu, G. Pastore, M. Tonks, P. Millett, B. Dorado, D. Gaston, D. Andrs, R. Williamson, R. Martineau, B. Uberuaga, C. Stanek, Atomistic modeling of intrinsic and radiation-enhanced fission gas (Xe) diffusion in $UO_{2\pm x}$: Implications for nuclear fuel performance modeling, J. Nucl. Mater. 451 (2014) 225–242.

[17] D. A. Andersson, B. P. Uberuaga, P. V. Nerikar, C. Unal, C. R. Stanek, U and Xe transport in $UO_{2\pm x}$: Density functional theory calculations, Phys. Rev. B 84 (2011) 054105.

[18] C. Matthews, R. Perriot, M. W. Cooper, C. R. Stanek, D. A. Andersson, Cluster dynamics simulation of uranium self-diffusion during irradiation in UO_2, J. Nucl. Mater. 527 (2019) 151787.

[19] W. Setyawan, M. W. D. Cooper, K. J. Roche, R. J. Kurtz, B. P. Uberuaga, D. A. Andersson, B. D. Wirth, Atomistic model of xenon gas bubble re-solution rate due to thermal spike in uranium oxide, J. Appl. Phys. 124 (2018) 075107.

[20] D. Xu, B. D. Wirth, Modeling spatially dependent kinetics of helium desorption in bcc iron following he ion implantation, Journal of Nuclear Materials 403 (2010) 184–190.

[21] B. D. Wirth, X. Hu, A. Kohnert, D. Xu, Modeling defect cluster evolution in irradiated structural materials: Focus on comparing to high-resolution experimental characterization studies, J. Mater. Res, 30 (2015) 1440–1455.

[22] D. Maroudas, S. Blondel, L. Hu, K. D. Hammond, B. D. Wirth, Helium segregation on surfaces of plasma-exposed tungsten, J. Condens. Matter Phys. 28 (2016) 064004.

[23] S. Blondel, D. E. Bernholdt, K. D. Hammond, B. D. Wirth, Continuum-scale modeling of helium bubble bursting under plasma-exposed tungsten surfaces, Nucl. Fusion 58 (2018) 126034.

[24] S. Blondel, D. E. Bernholdt, K. D. Hammond, L. Hu, D. Maroudas, B. D. Wirth, Benchmarks and tests of a multidimensional cluster dynamics model of helium implantation in tungsten, Fusion Sci. Technol. 71 (2017) 84–92.

[25] T. Barani, G. Pastore, A. Magni, D. Pizzocri, P. Van Uffelen, L. Luzzi, Modeling intra-granular fission gas bubble evolution and coarsening in uranium dioxide during in-pile transients, J. Nucl. Mater. 538 (2020) 152195.

[26] D. Pizzocri, G. Pastore, T. Barani, A. Magni, L. Luzzi, P. Van Uffelen, S. Pitts, A. Alfonsi, J. Hales, A model describing intra-granular fission gas behaviour in oxide fuel for advanced engineering tools, J. Nucl. Mater. 502 (2018) 323–330.

[27] M. R. Tonks, D. Gaston, P. C. Millett, D. Andrs, P. Talbot, An object-oriented finite element framework for multiphysics phase field simulations, Comput. Mater. Sci. 51 (2012) 20.

[28] M. W. Cooper, G. Pastore, Y. Che, C. Matthews, A. Forslund, C. R. Stanek, K. Shirvan, T. Tverberg, K. A. Gamble, B. Mays, D. A. Andersson, Fission gas diffusion and release for Cr_2O_3-doped UO_2: From the atomic to the engineering scale, J. Nucl. Mater. 545 (2021) 152590.

[29] C. J. Permann, D. R. Gaston, D. Andrš, R. W. Carlsen, F. Kong, A. D. Lindsay, J. M. Miller, J. W. Peterson, A. E. Slaughter, R. H. Stogner, R. C. Martineau, Moose: Enabling massively parallel multiphysics simulation, SoftwareX 11 (2020) 100430.

[30] D.-U. Kim, S. Blondel, D. E. Bernholdt, P. Roth, F. Kong, D. Andersson, M. R. Tonks, B. D. Wirth, Modeling mesoscale fission gas behavior in UO_2 by directly coupling the phase field method to spatially resolved cluster dynamics (2021).

[31] L. K. Aagesen, D. Schwen, M. R. Tonks, Y. Zhang, Phase-field modeling of fission gas bubble growth on grain boundaries and triple junctions in UO_2 nuclear fuel, Comp. Mater. Sci. 161 (2019) 35–45.

[32] M. F. Adams, J. Brown, P. Brune, K. Buschelman, L. Dalcin, V. Eijkhout, W. D. Gropp, D. Kaushik, M. G. Knepley, D. A. May, L. C. McInnes, R. T. Mills, T. Munson, K. Rupp, P. Sanan, B. F. Smith, S. Zampini, H. Zhang, H. Zhang, Petsc users manual, Tech. rep., Argonne National Laboratory (2020).

[33] C. J. Permann, M. R. Tonks, B. Fromm, D. R. Gaston, Order parameter re-mapping algorithm for 3d phase field model of grain growth using fem, Comp. Mater. Sci. 115 (2016) 18–25.

[34] D. R. Gaston, C. J. Permann, J. W. Peterson, A. E. Slaughter, D. Andrš, Y. Wang, M. P. Short, D. M. Perez, M. R. Tonks, J. Ortensi, L. Zou, R. C. Martineau, Physics-based multiscale coupling for full core nuclear reactor simulation, Ann. Nucl. Energy 84 (2015) 45–54.

[35] G. Pastore, M3MS-18IN0101092: Develop and implement in the bison code a new engineering model for intra-granular fission gas behavior in uranium dioxide, Tech. rep., Idaho National Laboratory (2018).

[36] G. Pastore, et al., Modeling intra-granular fission gas bubble evolution applied to engineering analyses (M3MS-20IN0101062), Tech. rep., Idaho National Laboratory (2020).

[37] T. Kogai, Modelling of fission gas release and gaseous swelling of light water reactor fuels, J. Nucl. Mater. 244 (1997) 131–140.

[38] B. Debusschere, H. Najm, P. Pébay, O. Knio, R. Ghanem, O. Le Maître, Numerical challenges in the use of polynomial chaos representations for stochastic processes, SIAM J Sci Comput. 26 (2004) 698–719.

[39] B. Debusschere, K. Sargsyan, C. Safta, K. Chowdhary, The uncertainty quantification toolkit (UQTk), in: R. Ghanem, D. Higdon, H. Owhadi (Eds.), Handbook of Uncertainty Quantification, Springer, 2017, pp. 1807–1827.

[40] D. Xiu, G. E. Karniadakis, The wiener–askey polynomial chaos for stochastic differential equations, SIAM J Sci Comput. 24 (2002) 619–644.

[41] R. White, M. Tucker, A new fission-gas release model, J. Nucl. Mater. 118 (1983) 1–38.